PERGAMON

International Journal of Heat and Mass Transfer 45 (2002) 865–875

International Journal of HEAT and MASS TRANSFER

www.elsevier.com/locate/ijhmt

Numerical analysis for photothermal poling process of nonlinear optical polymer film

Hiroaki Kobayashi, Masaki Kubo, Takao Tsukada *, Mitsunori Hozawa

Institute of Multidisciplinary Research for Advanced Materials, Tohoku University, Katahira 2-1-1, Aoba-ku, Sendai 980-8577, Japan

Received 1 November 2000; received in revised form 23 March 2001

Abstract

Numerical simulations of the manufacturing of waveguides with grating patterns on a nonlinear optical (NLO) polymer film using photothermal poling were carried out. The mathematical model was constructed, in which spatial and temporal variations of molecular dipoles during heating with a focused laser beam and electrical poling were considered. The effects of operational factors, i.e., laser power, beam diameter, moving speed of a sample, and electric field strength, on the grating configuration were investigated. As a result, the following guidelines for producing a waveguide with high performance were obtained. The laser beam wavelength should be selected so as to heat uniformly throughout the thickness of the polymer film, the laser power should be as high as possible without causing large deformation in the film, the laser beam diameter should be smaller than half period of the grating, the moving speed of the stage should be slow, and the electric field strength should be as high as possible, if dielectric breakdown is to be avoided.

1. Introduction

In recent years, a large number of nonlinear optical (NLO) polymers have been developed for optical devices such as waveguides [1] and optical modulators [2], and for optical applications such as optical memory storage [3] and holography [4]. Conventionally, inorganic crystals have been used as materials for such devices and applications because of their high NLO performance. However, long period of time and delicate control are required to grow high-quality crystals with large diameter. On the other hand, NLO polymers have excellent potential and benefits [5], i.e., in versatility and ease of fabrication as well as the large NLO susceptibilities of the molecules embedded in the polymers.

In order to generate second-order NLO properties in glassy polymers, it is necessary that the suitable NLO molecules, chromophores, are doped into or functionalized onto the polymers. Then, electric field poling must be applied, while heating the materials over their glass transition temperature (T_g), in order to align the dipoles of the NLO molecules in the electric field and achieve the non-centrosymmetric ordering of the molecules [6,7]. The magnitude of second-order nonlinearity of the poled polymers depends on the number density of NLO molecules, and their degree of the orientational order.

Recently, a photothermal poling process for fabricating a channel waveguide on a NLO polymer thin film has been proposed [8,9]. The NLO polymer film on a moving stage is illuminated with a focused laser beam for local heating over T_g, and simultaneously an electric field is applied across the film sandwiched between two electrodes, so that the molecular dipoles can be oriented in the form of the channel. This method is very simple and inexpensive because it does not need to make channel-patterned electrodes on the sample by photolithography or heat the entire sample over T_g. In addition, by periodically switching the direction of the electric field as shown in Fig. 1, photothermal poling can yield alternate dipole orientation gratings suitable for quasiphase matching (QPM) in wavelength conversion devices. According to Yilmaz et al. [8], the wavelength converter with high efficiency requires the rectangular

* Corresponding author. Tel.: +81-22-217-5651; fax: +81-22-217-5651.

E-mail address: tsukada@tagen.tohoku.ac.jp (T. Tsukada).

0017-9310/02/$ - see front matter
PII: S0017-9310(01)00156-9

Nomenclature

C_P	specific heat
d_{laser}	diameter of laser beam
D_R	rotational diffusion coefficient
E	electric field strength
ΔE_{act}	activation energy
f	square-wave frequency of electric field
$f^{\omega}, f^{2\omega}$	local field factor
$f(\theta, t)$	distribution function
k	Boltzmann constant
n	number of time-steps
N	number density of chromophore
Q	laser power
R	gas constant
T	time
Δt	time increment
T	temperature
T_a	atmospheric temperature
T_g	glass transition temperature
u	moving speed of stage
$V(\theta, t)$	potential energy
X, Y, Z	coordinates

Greek symbols

α	reflectance
β	absorption coefficient
β_{333}	molecular hyperpolarizability
χ	electric susceptibility
ϕ	azimuthal angle
λ	thermal conductivity
μ	permanent dipole
θ	polar angle between poling electric field and molecular dipole
ρ	density

Subscripts

clad	cladding layer
glass	glass substrate
poly	NLO polymer
stage	moving stage

dipole orientation grating at regular intervals in the NLO polymer film as shown in Fig. 1, but the grating may become sinusoidal rather than rectangular, depending on the operational parameters such as the power and diameter of the laser beam, the moving speed of the stage and the modulation frequency of the electric field, because of thermal diffusion during the poling. Therefore, it is necessary to determine the optimal operational conditions to make the configuration of grating rectangular, but there have been no report in which an optimization was carried out yet.

In the photothermal poling process, it is very important to understand the heat transfer and the dynamics of the molecular dipole orientation in polymer films with doped or covalently linked NLO molecules, during laser beam heating and electric field poling, because these phenomena determine the spatial resolution of the channel waveguide, i.e., the performance of the

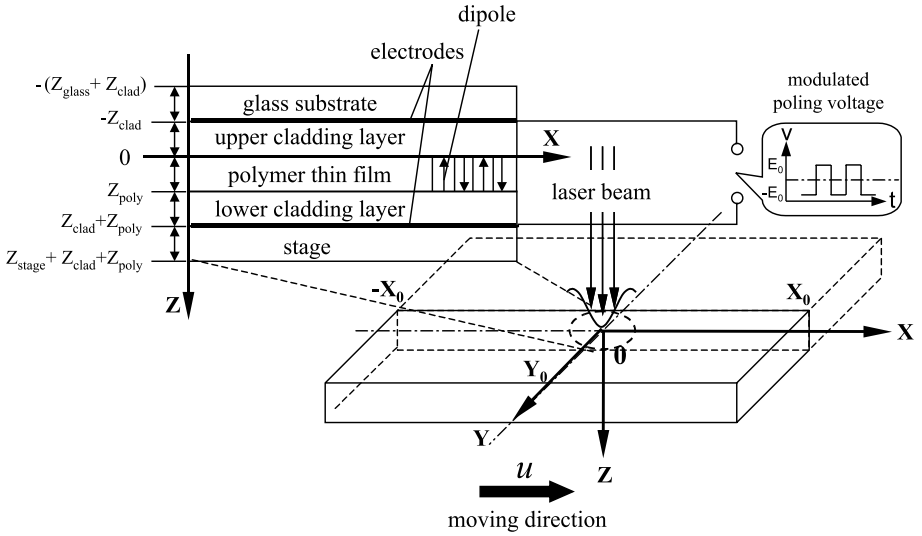

Fig. 1. Schematic illustration of photothermal poling process.

devices. In this work, we construct a mathematical model of the manufacturing of channel waveguides with grating patterns on a NLO polymer film by the photothermal poling process, in which spatial and temporal variations of dipole orientation during heating and electrical poling are considered. Then, the effects of the operational factors of the process, such as the laser beam diameter, the moving speed of the stage and the electric field strength, are investigated in order to seek the optimal operational conditions to make the periodic dipole grating rectangular.

2. Numerical analysis of photothermal poling process

2.1. Temperature distributions in NLO polymer thin films

Fig. 1 shows a schematic illustration of the physical model of the photothermal poling process used in the numerical simulation. The system consists of a glass substrate, a NLO polymer film sandwiched between polymeric cladding layers, two electrodes and a metallic moving stage. The two electrodes are transparent and their thicknesses are considered to be infinitesimal. The stage moves in the X direction at a speed u μm/s. The laser beam enters the medium from the $-Z$ direction, and its center passes through the origin. Because the system is symmetrical on a X–Z plane, half of the system is set as the analytical region.

The following assumptions are introduced in the model: (1) the system is in a steady state; (2) the calculation domain, i.e., near the region irradiated by the laser beam, is far from the edge of the device, and thus the edge effect is negligible; (3) the laser beam passing through the NLO polymer thin film is completely absorbed in the moving stage; (4) the intensity distribution of the laser beam is an axis-symmetric Gaussian distribution.

Under the above assumptions, the governing equation, i.e., the three-dimensional energy equation is described as follows:

$$\frac{\partial}{\partial X}(\rho_i C_{\mathrm{P}i} u T_i) = \left\{ \frac{\partial}{\partial X}\left(\lambda_i \frac{\partial T_i}{\partial X}\right) + \frac{\partial}{\partial Y}\left(\lambda_i \frac{\partial T_i}{\partial Y}\right) + \frac{\partial}{\partial Z}\left(\lambda_i \frac{\partial T_i}{\partial Z}\right) \right\} + \frac{\beta_i (1-\alpha) Q_i}{\pi (d_{\mathrm{laser}}/2)^2} \times \exp\left(-\frac{2(X^2+Y^2)}{(d_{\mathrm{laser}}/2)^2} \right), \tag{1}$$

where

$$Q_i = \begin{cases} Q \exp\left(-\beta_{\mathrm{glass}}(Z + Z_{\mathrm{glass}} + Z_{\mathrm{clad}})\right) \\ \quad (i = \mathrm{glass}), \\ Q \exp\left(-\beta_{\mathrm{glass}} Z_{\mathrm{glass}} - \beta_{\mathrm{clad}}(Z + Z_{\mathrm{clad}})\right) \\ \quad (i = \mathrm{clad(upper)}), \\ Q \exp\left(-\beta_{\mathrm{glass}} Z_{\mathrm{glass}} - \beta_{\mathrm{clad}} Z_{\mathrm{clad}}\right) \exp\left(-\beta_{\mathrm{poly}} Z\right) \\ \quad (i = \mathrm{poly}), \\ Q \exp\left(-\beta_{\mathrm{glass}} Z_{\mathrm{glass}} - \beta_{\mathrm{clad}} Z_{\mathrm{clad}} - \beta_{\mathrm{poly}} Z_{\mathrm{poly}}\right) \\ \times \exp\left(-\beta_{\mathrm{clad}}(Z - Z_{\mathrm{poly}})\right) \\ \quad (i = \mathrm{clad(lower)}), \\ Q \exp\left(-\beta_{\mathrm{glass}} Z_{\mathrm{glass}} - \beta_{\mathrm{clad}} Z_{\mathrm{clad}} - \beta_{\mathrm{poly}} Z_{\mathrm{poly}}\right) \\ \times \exp\left(-\beta_{\mathrm{clad}}(Z - Z_{\mathrm{poly}} - Z_{\mathrm{clad}})\right) \\ \quad (i = \mathrm{stage}). \end{cases}$$

The left-hand side of Eq. (1) denotes the convective heat transfer due to the movement of the stage. The second term on the right-hand side denotes heat generation by absorption of the laser beam. The boundary conditions are described as follows:

$$\frac{\partial T_i}{\partial Y} = 0 \quad (Y = 0), \tag{2.1}$$

$$T_{\mathrm{clad}} = T_{\mathrm{glass}}, \qquad \lambda_{\mathrm{clad}} \frac{\partial T_{\mathrm{clad}}}{\partial Z} = \lambda_{\mathrm{glass}} \frac{\partial T_{\mathrm{glass}}}{\partial Z} \quad (Z = -Z_{\mathrm{clad}}), \tag{2.2, 3}$$

$$T_{\mathrm{clad}} = T_{\mathrm{poly}}, \qquad \lambda_{\mathrm{clad}} \frac{\partial T_{\mathrm{clad}}}{\partial Z} = \lambda_{\mathrm{poly}} \frac{\partial T_{\mathrm{poly}}}{\partial Z} \quad (Z = 0, Z_{\mathrm{poly}}), \tag{2.4, 5}$$

$$T_{\mathrm{clad}} = T_{\mathrm{stage}}, \qquad \lambda_{\mathrm{clad}} \frac{\partial T_{\mathrm{clad}}}{\partial Z} = \lambda_{\mathrm{stage}} \frac{\partial T_{\mathrm{stage}}}{\partial Z} \quad (Z = Z_{\mathrm{clad}} + Z_{poly}), \tag{2.6, 7}$$

$$T = T_{\mathrm{a}} \qquad (X = X_0, -X_0,\ Y = Y_0,\ Z = -(Z_{\mathrm{clad}} + Z_{\mathrm{glass}}),\ Z_{\mathrm{poly}} + Z_{\mathrm{clad}} + Z_{\mathrm{stage}}). \tag{2.8}$$

The above governing equation and the boundary conditions are discretized by a control volume method using non-uniform grids ($128 \times 50 \times 85$) to increase the resolution of the domain irradiated by the laser beam.

Tables 1 and 2 show size of the analytical region and physical properties of the materials used in the numerical simulation. The glass substrate and the moving stage are considered to be made of Pyrex 7740 and aluminium [10], respectively. In addition, the NLO polymer is considered to be poly(methyl methacrylate) (PMMA) [10], as well as the cladding layers, because of no

Table 1
Size of analytical region

$2X_0$ (μm)	Y_0 (μm)	Z_{glass} (μm)	Z_{clad} (μm)	Z_{poly} (μm)	Z_{stage} (μm)
333	162	93	3	3	93

Table 2
Physical properties of materials used in the numerical simulation

		ρ (kg/m^3)	C_P (J/kg K)	λ (W/m K)
Glass	(Pyrex7740)	2.23×10^3	0.73×10^3	1.10
Clad layer	(PMMA)	1.19×10^3	1.47×10^3	2.10×10^{-1}
Polymer	(PMMA)	1.19×10^3	1.47×10^3	2.10×10^{-1}
Stage	(Al)	2.70×10^3	0.90×10^3	2.37×10^2
α	β(glass, cladding layer) (m^{-1})	β(stage) (m^{-1})	T_a (K)	T_g (K)
0.1	1.60×10^2	1.00×10^7	300	407

available data for the thermophysical properties of the NLO polymers. PMMA is commonly used as a polymer matrix of NLO polymer film.

The size of the actual device is on the millimeter scale. The laser beam diameter irradiating the polymer thin film (1–10 μm) and the thickness of the film (3 μm) are on the micrometer scale. It is practically difficult to discretize the entire system on the millimeter scale with the control volumes on the micrometer scale, because a large number of control volumes are needed. Thus, the calculated domain is reduced to near the region illuminated by the laser beam ($333 \times 162 \times 195$ μm^3), and the temperature at the boundary is assumed to be the atmospheric temperature (300 K). To check the validity of this boundary condition, the calculations were carried out when domains were changed with twice and the three times of volumes, and it was confirmed that the temperature profile does not change.

2.2. Dynamics of dipole orientation of NLO molecules

The temperature field in the device shown in Fig. 1 is in a steady state, because it is considered in the stationary coordinates, i.e., the coordinates fixed with the laser irradiation. However, the dipole orientation of NLO molecules at a certain point in the polymer film varies with time, depending on the thermal history due to the movement of the stage and on the time variation of the electric field across the film. In the present work, the transient variation of the dipole orientation of NLO molecules in the polymer film is described by a three-dimensional rotational diffusion model [11–13], where the molecule is considered to be a rigid rod with a permanent dipole μ, as shown in Fig. 2. Solid lines indicate the laboratory coordinate axes (X, Y, Z). Dashed lines indicate the molecular principal axes (1,2,3), where the three-axis is the molecular symmetry axis. The poling electric field is applied along the Z-axis. θ is the spherical polar angle between the electric field E and the principal three-axis of the molecule, and ϕ is the azimuthal angle.

In the presence of the electric field, the rotational diffusion equation of the NLO molecule characterized by a rigid rod is given by the following Smoluchowski equation [14,15]:

$$\frac{1}{D_R(T)}\frac{\partial f(\theta,t)}{\partial t} = \frac{1}{\sin\theta}\frac{\partial}{\partial\theta}\left[\sin\theta\left\{\frac{\partial f(\theta,t)}{\partial\theta}+\frac{f(\theta,t)}{kT}\frac{\partial V(\theta,t)}{\partial\theta}\right\}\right], \quad (3)$$

where the distribution function $f(\theta,t)$ represents the probability distribution of obtaining the molecular dipole vector at orientation θ at time t. $D_R(T)$ is the rotational diffusion coefficient, and is approximated by Eq. (4), being based on the measured values of *N*-(4-nitrophenyl)-(*s*)-protinoxy poly(*p*-hydroxystyrene) [13], because there are no available data of D_R except for this material.

$$D_R(T) = 3.96 \times 10^{12}\exp\left(-\frac{\Delta E_{act}}{RT}\right)\ [\mathrm{rad}^2/\mathrm{s}] \quad (\Delta E_{act} = 116\ \mathrm{kJ/mol}). \quad (4)$$

$V(\theta,t)$ is the potential energy of the permanent dipole μ in the electric field $E(t)$, and is given as follows:

$$V(\theta,t) = -\mu E(t)\cos\theta, \quad (5)$$

where $E(t)$ is given as the electric field in the NLO polymer film, and the field in the cladding layers is not taken into account.

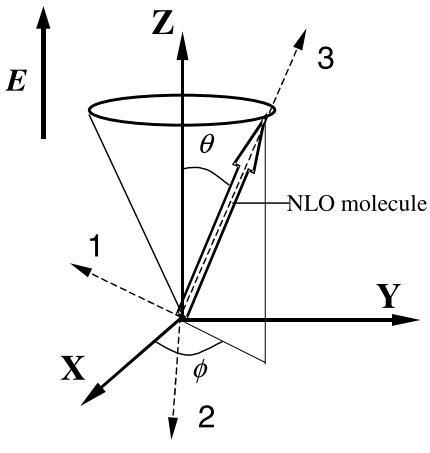

Fig. 2. Three-dimensional rotational diffusion model of polar molecule in the presence of an external field.

If the polymer is assumed to be initially amorphous and there is no external field at $t < 0$, the initial condition can be stated as $f = 1/2$, since normalization of the probability over the hemisphere requires that

$$\int_{-1}^{1} f(\theta, t)\,\mathrm{d}\cos\theta = 1. \tag{6}$$

The boundary condition can be represented as a set of "no-flux" condition,

$$\frac{\mathrm{d}f(\theta, t)}{\mathrm{d}\theta} = 0 \quad (\theta = 0, \pi). \tag{7}$$

The magnitude of the macroscopic NLO effect induced by an external electric field is determined by the number density of the NLO molecules within the polymer film and their degree of the dipole orientation order. Eq. (8) indicates the relation between the macroscopic second-order susceptibility tensor, $\chi^{(2)}_{ZZZ}$, and the angular average, $\langle\cos^3\theta\rangle$, which describes the degree of dipole orientation during poling [16],

$$\chi^{(2)}_{ZZZ} = N\beta_{333} f^{\omega} f^{\omega} f^{2\omega} \langle\cos^3\theta\rangle, \tag{8}$$

where f^{ω} and $f^{2\omega}$ are the local field factors which are a function of the frequency of the optical field, ω. N is the number of NLO molecules which are allowed to rotate. β_{333} is a component of the molecular hyperpolarizability tensor, $\boldsymbol{\beta}$. The angular average, $\langle\cos^3\theta\rangle$, is given with the distribution function $f(\theta, t)$ as follows:

$$\langle\cos^3\theta\rangle = \frac{\int_{-1}^{1} f(\theta, t)\cos^3\theta\,\mathrm{d}\cos\theta}{\int_{-1}^{1} f(\theta, t)\,\mathrm{d}\cos\theta}. \tag{9}$$

The initial value problems, Eqs. (3)–(9), describe the transient behavior of the dipole orientation of a NLO molecule at an arbitrary point in the NLO polymer film after the electric field is applied across the film, if the thermal history of the NLO molecule is given and then the rotational diffusion coefficient $D_{\mathrm{R}}(T)$ is estimated using Eq. (4). Eqs. (3)–(7) are solved by use of the finite difference method, and the calculations of the integrals in Eq. (9) are carried out numerically with a trapezoidal rule.

Fig. 3 shows the flow diagram of the numerical simulation of transient behavior of a NLO molecule that is initially at point (X, Y, Z) in the polymer film. The initial temperature of the molecule is the temperature at point (X, Y, Z) obtained by steady-state thermal analysis in Section 2.1. First, the initial condition is set. Next, the temperature of the NLO molecule at time $t = \Delta t$ is determined such that it is the same as that at point $(X + u\Delta t, Y, Z)$ in the steady-state temperature distributions, because the NLO molecule moves $u\Delta t$ in the X direction due to the movement of the stage. Using the mean value of $T(X, Y, Z)$ and $T(X + u\Delta t, Y, Z)$, the rotational diffusion coefficient D_{R} is estimated by Eq. (4),

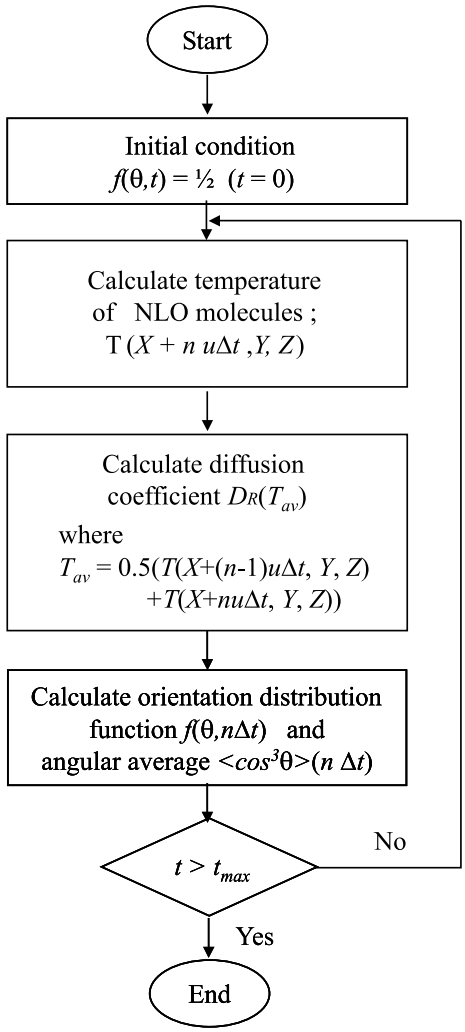

Fig. 3. Flow diagram of numerical analysis for transient behavior of NLO molecules.

and then the distribution function and the angular average at time $t = \Delta t$ are calculated using Eqs. (3) and (9). The above steps are repeated for the NLO molecules at all points in the film until $t = t_{\max}$.

3. Results and discussion

3.1. Distributions of temperature and molecular dipole orientation in NLO polymer film

Fig. 4 shows the time variations of: (a) temperature, (b) electric field and (c) angular average of NLO molecules which are initially at points (X, Y, Z) in a polymer film, where the film is mounted on a stage moving at 5.0×10^{-2} μm/s and is locally illuminated by a laser

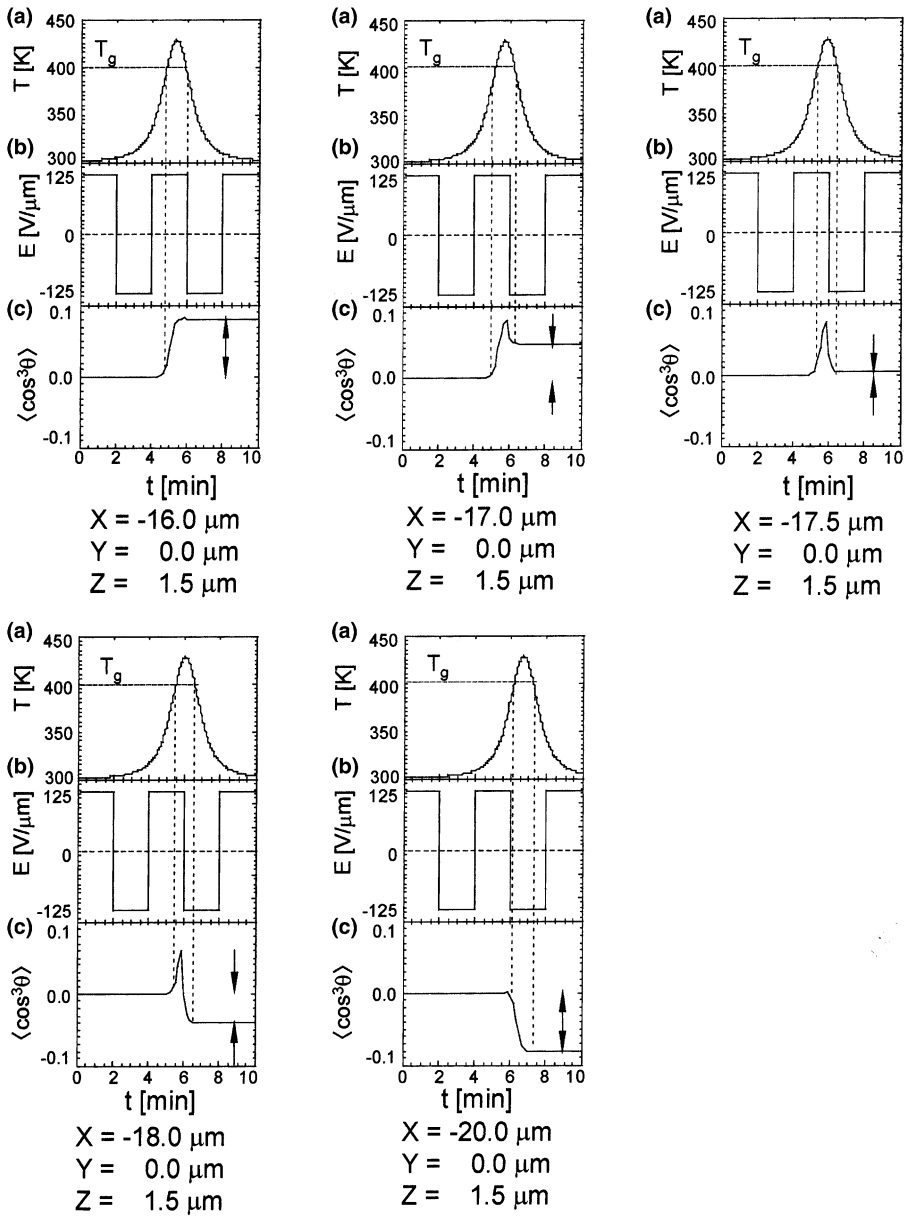

Fig. 4. Time variations of: (a) temperature, (b) the electric field, and (c) angular average of NLO molecules at several points. $u = 5 \times 10^{-2}$ μm/s ($f = 4.17 \times 10^{-3}$ Hz), $d_{laser} = 6$ μm, $E = 125$ V/μm, $Q = 7$ mW.

with a diameter of 6 μm and power of 7 mW. The absorption coefficient of the polymer film is 7.4×10^4 m^{-1}, which corresponds to β of PMMA with 30 mol% Disperse Red 1 as the NLO molecule at 632 nm of a He–Ne laser beam. The electric field applied across the film is 125 V/μm, and the direction is periodically inversed at frequency of 4.17×10^{-3} Hz, as shown in Fig. 4(b). The poling electric field strength applied to align the NLO molecules is generally in the range of 20–130 V/μm [4–9,12,13]. The temperature variations in Fig. 4(a) are calculated based on the steady-state temperature distribution in the polymer film, as described in Section 2.1. The temperature of each NLO molecules rises gradually as it approaches the region irradiated by the laser, and then falls after passing through the region. Since the NLO molecule can easily move over the glass transition temperature T_g, which is set at T_g of *N*-(4-nitrophenyl)-(*s*)-protinoxy poly(*p*-hydroxystyrene), i.e., 407 K, in this work and is indicated by dashed lines in Fig. 4, the dipole of the molecule is first oriented depending on the

direction of the electric field, and its absolute value increases with the temperature. Then, when the electric field is inversed above T_g, the molecular dipole is also oriented in the opposite direction. However, the degree of the dipole orientation is restricted to a certain limit because the mobility of the molecular dipole decreases rapidly below T_g. Finally, the degree of dipole orientation indicated by arrows in Fig. 4(c) is maintained at each position.

Fig. 5 shows the distributions of temperature and angular average $\langle\cos^3\theta\rangle$ in the NLO polymer film for two different values of the absorption coefficient, i.e., 7.4×10^4 and 1.0×10^6 m^{-1}, where the former corresponds to β of PMMA with 30 wt% Disperse Red 1 at 632 nm of a He–Ne laser, and the latter, at 488 nm of an Ar^+ laser. The temperature distributions, which are solutions of the three-dimensional steady-state energy equations as described in Section 2.1, are obtained at the time when the polymer film is irradiated by the laser beam, while the distributions of angular average are obtained at the time when the laser beam is turned off and the polymer is cooled to almost atmospheric temperature, T_a. Thus, the angular averages at several points in the figure correspond to the final state of $\langle\cos^3\theta\rangle$ in

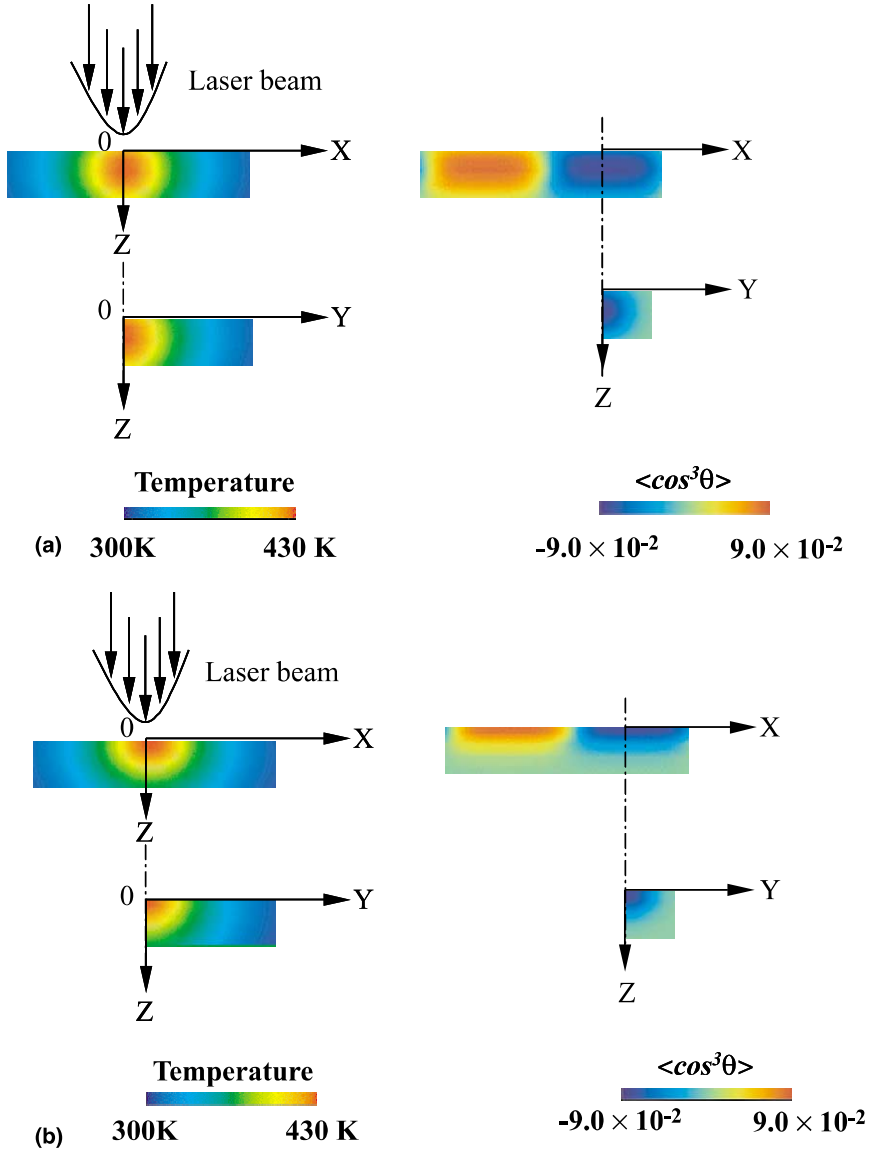

Fig. 5. Distributions of temperature and angular average $\langle\cos^3\theta\rangle$ in the NLO polymer film for two different values of absorption coefficient: (a) $\beta = 7.4 \times 10^4$ m^{-1}, (b) $\beta = 1.0 \times 10^6$ m^{-1}. $u = 5 \times 10^{-2}$ μm/s ($f = 4.17 \times 10^{-3}$ Hz), $d_{laser} = 6$ μm, $E = 125$ V/μm, $Q =$ 7 mW ($\beta = 7.4 \times 10^4$ m^{-1}), 1.4 mW ($\beta = 1.0 \times 10^6$ m^{-1}).

Fig. 4(c). The beam diameter of the laser is fixed at 6 μm, but the laser power is adjusted to: (a) 7.0 mW and (b) 1.4 mW so that the maximum value of the angular average in the polymer films is approximately 9.0×10^{-2}. If the same power as that of the Ar^+ laser beam, 1.4 mW, is used, the temperature throughout the polymer film will be below T_g and the orientation of molecular dipoles by means of the He–Ne laser will not occur at all. In Fig. 5, the remaining operational parameters are the same as those in Fig. 4. Since the angular average describes the degree of the molecular dipole orientation, the distributions in the X–Z plane represent the configurations of the dipole orientation grating and those in the Y–Z plane determine the spatial resolution of the cross-section of the waveguide. The combination of the moving speed with the frequency of the electric field used here ideally produces a rectangular dipole orientation grating of 6 μm throughout the film thickness. However, the grating of the angular average appears in both X–Z and Y–Z planes, because of diffusion of thermal energy. In particular, the blurred boundary between domains with the opposite polarities in the X–Z plane is due to the reorientation of the dipole, which has already been oriented, to the opposite direction, as shown in Fig. 4.

In addition, a comparison of the results for different absorption coefficients reveals that the photothermal poling using a laser with a wavelength, at which the absorption coefficient of the NLO polymer is low, leads to a polymer film with a more uniform distribution of the dipole orientation throughout the thickness.

3.2. Effects of operational factors on dipole orientation grating

In the present work, to investigate the effects of various operational factors on the dipole orientation grating, the average value of $\langle \cos^3 \theta \rangle$ throughout the film thickness, i.e., $\langle \overline{\cos^3 \theta} \rangle$ as defined by the following equation, is calculated in both X and Y directions:

$$\langle \overline{\cos^3 \theta} \rangle = \frac{1}{Z_{\text{poly}}} \int_0^{Z_{\text{poly}}} \langle \cos^3 \theta \rangle \, dZ. \tag{10}$$

Fig. 6 shows the effect of laser power on the distributions of $\langle \overline{\cos^3 \theta} \rangle$ in the (a) X and (b) Y directions, where two cycles of the distributions of $\langle \overline{\cos^3 \theta} \rangle$ in the X direction are shown in Fig. 6(a). Fig. 6(b) shows the distributions in the Y direction at X = 3 μm in Fig. 6(a). The diameter of the laser beam is fixed at 6 μm. The absorption coefficient of the polymer film at the wavelength of the laser is assumed to be 7.4×10^4 m^{-1}. The electric field applied across the film is 125 V/μm, and the direction is periodically inversed at the frequency of 4.17×10^{-3} Hz. Thus, the half period of the grating is estimated to be 6 μm using the speed of the stage,

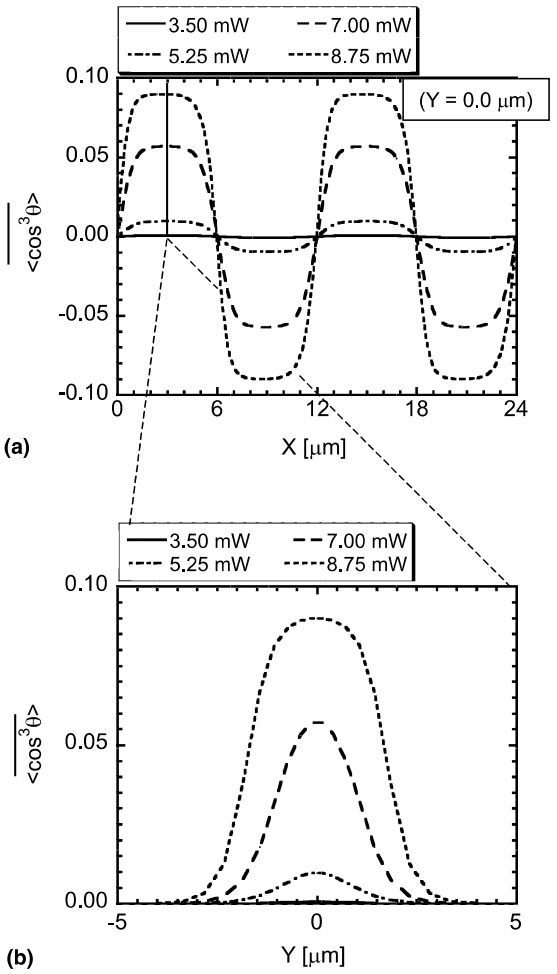

Fig. 6. Effect of laser power on grating configurations in: (a) X and (b) Y directions, $u = 5 \times 10^{-2}$ μm/s ($f = 4.17 \times 10^{-3}$ Hz), $d_{\text{laser}} = 6$ μm, $E = 125$ V/μm.

5×10^{-2} μm/s. The absolute value of $\langle \overline{\cos^3 \theta} \rangle$, which describes the degree of dipole orientation, increases in both X and Y directions as the laser power increases. This is because the average temperature near the area illuminated by laser increases with the laser power, and consequently, the time for which the temperature is kept above T_g and the molecular dipole can rotate easily becomes longer.

Fig. 7 shows the effect of the diameter of the laser beam on the configurations of the dipole orientation grating, where the laser power is 7 mW and the other operational parameters are the same as those in Fig. 6. For a given the half period of the grating, i.e., 6 μm, which is determined by both the speed of the stage and the frequency of the electric field, the grating configurations become more rectangular and the absolute value of $\langle \overline{\cos^3 \theta} \rangle$ increases as the beam diameter decreases. Since the intensity of the laser beam, i.e., $Q/\pi d_{\text{laser}}^2$,

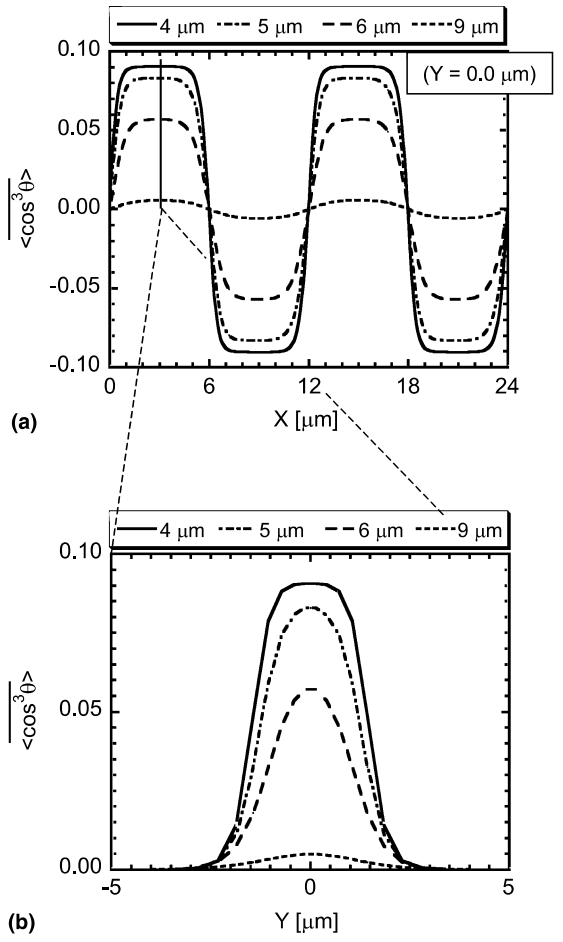

Fig. 7. Effect of diameter of laser beam on the grating configurations in: (a) X and (b) Y directions. $u = 5 \times 10^{-2}$ μm/s ($f = 4.17 \times 10^{-3}$ Hz), $E = 125$ V/μm, $Q = 7$ mW.

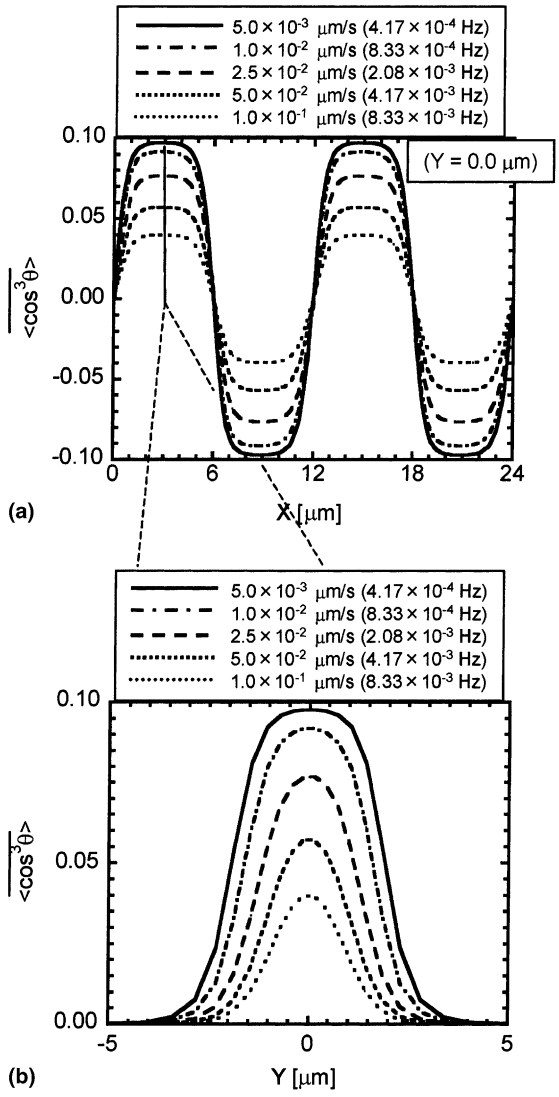

Fig. 8. Effect of moving speed on grating configurations in: (a) X and (b) Y directions. $d_{\text{laser}} = 6$ μm, $E = 125$ V/μm, $Q = 7$ mW.

increases as the beam diameter decreases and the temperature gradient along the moving direction of the stage, i.e., X direction, becomes steeper, the time for the reorientation process of the already oriented dipole described in Section 3.1 becomes shorter. This leads to more rectangular configuration of the grating. However, the width of the waveguide remains almost unchanged due to the reduction of the beam diameter and increase of the intensity of the laser, as shown in Fig. 7(b).

Fig. 8 shows the effect of the moving speed of the stage on the grating configurations, where the laser power is 7 mW. The frequencies of the electric field are adjusted so that the half period of the grating may be 6 μm, but the other operational parameters are fixed to be the same values as those in Fig. 6. The absolute value of $\langle\overline{\cos^3\theta}\rangle$, i.e., the degree of dipole orientation, increases throughout the film as the moving speed decreases. For a given grating period, the slower the moving speed, the longer the time for which the temperature is kept above T_g, and therefore the molecular dipole can orient easily.

Fig. 9(a) shows the time variation of the average temperature of the NLO molecules, which travel on the X–Z plane ($Y = 0$) with the moving stage, throughout the polymer film thickness. In the figure, $T_{\max}$ is the maximum value of the temperature, and T_m is an arithmetic mean between $T_{\max}$, and glass transition temperature, T_g. t_m shows the time for which the temperature of the NLO molecules is kept above T_g. Considering that t_m is the characteristic time for heating of the NLO polymer film and $1/D_R(T_m)$ is the characteristic time for poling, the relation between the maximum value of $\langle\overline{\cos^3\theta}\rangle$ in the NLO polymer film and the ratio of these

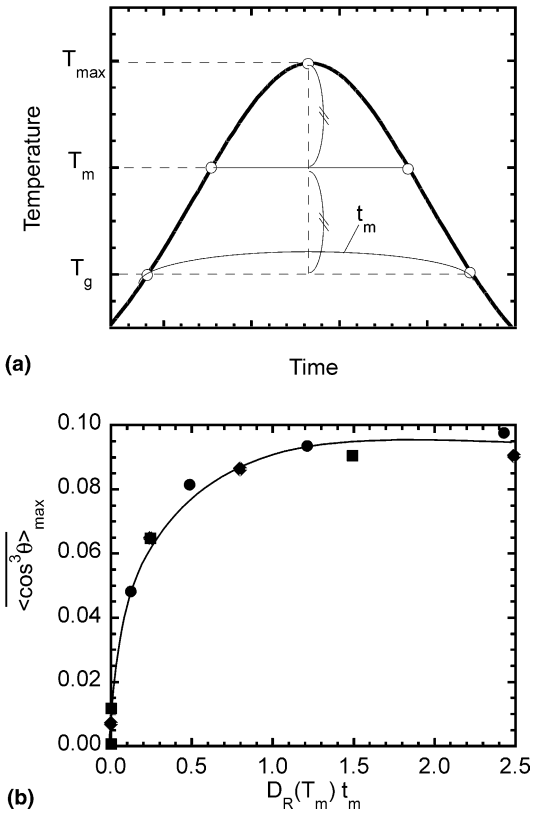

Fig. 9. Relation between $\langle\overline{\cos^3\theta}\rangle_{\max}$ and dimensionless number, $D_R(T_m)t_m$.

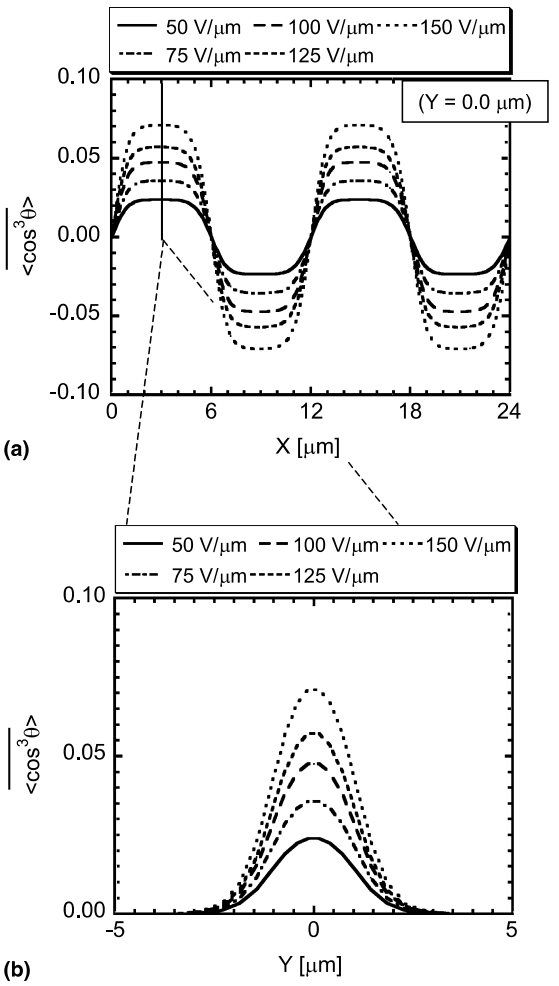

Fig. 10. Effect of electric field strength on grating configurations in: (a) X and (b) Y directions. $u = 5 \times 10^{-2}$ μm/s (4.17×10^{-3} Hz), $d_{laser} = 6$ μm, $Q = 7$ mW.

characteristic times, $D_R(T_m)t_m$, is given as shown in Fig. 9(b), where the results in the figure are based on those in Figs. 6–8. The maximum value of $\langle\overline{\cos^3\theta}\rangle$ which represents the degree of the dipole orientation increases with $D_R(T_m)t_m$, and becomes almost constant beyond a certain value of $D_R(T_m)t_m$, approximately unity.

Fig. 10 shows the effect of an electric field strength on the distributions of $\langle\overline{\cos^3\theta}\rangle$ in the (a) X and (b) Y directions, where the laser power is 7 mW and the other operational parameters are the same as those in Fig. 6. As the electric field strength increases, the absolute value of $\langle\overline{\cos^3\theta}\rangle$ increases throughout the film, because the external force causing the dipole orientation becomes stronger. Thus, the electric field strength should be high, if the dielectric breakdown is to be avoided

4. Conclusions

In this study, with the aim of controlling the dipole grating produced by the photothermal poling process, a mathematical model was constructed in which the spatial and temporal variations of molecular dipoles during laser heating and electric field poling were considered. Then, the effects of operational factors on the process were investigated numerically.

As a result, the following guidelines for the production of a waveguide with high performance were obtained: (1) the wavelength of the laser beam should be selected so as to heat uniformly across the thickness of NLO polymer films; (2) the beam diameter should be smaller than the half period of the dipole grating; (3) the moving speed of the stage should be relatively slow; (4) the electric field strength should be high, if the dielectric breakdown is to be avoided.

Acknowledgements

This research was partially supported by a Grant-in-Aid for Scientific Research (C)(2), 11650772, 1999–2000,

from the Ministry of Education, Science, Sports and Culture.

References

[1] D.M. Burland, R.D. Miller, O. Reiser, R.J. Twieg, C.A. Walsh, The design, synthesis, and evaluation of chromophores for second harmonic generation in a polymer waveguide, J. Appl. Phys. 71 (1992) 410–417.

[2] M. Hikita, Y. Shuto, M. Amano, R. Yoshimura, S. Tomaru, H. Kozawaguchi, Optical intensity modulation in a vertically stacked coupler incorporating electro-optic polymer, Appl. Phys. Lett. 63 (1993) 1161–1163.

[3] A. Natansohn, P. Rochon, J. Gosselin, S. Xie, Azo polymers for reversible optical storage. 1. Poly[4′-[[2-(acryloyloxy)ethyl]ethylamino]-4-nitroazobenzene], Macromolecules 25 (1992) 2268–2273.

[4] W.S. Baek, H. Lee, Photorefrective intermode space-charge fields in volume holographic interconnections, J. Appl. Phys. 67 (1990) 1194–1202.

[5] J.I. Thackara, G.F. Lipscomb, M.A. Stiller, A.J. Ticknor, R. Lytel, Poled electro-optic waveguide formation in thin-film organic media, Appl. Phys. Lett. 52 (1988) 1031–1033.

[6] G.R. Meredith, J.G. Van Dusen, D.J. Williams, Optical and nonlinear optical characterization of molecularly doped thermotropic liquid crystalline polymers, Macromolecules 15 (1982) 1385–1389.

[7] K.D. Singer, J.E. Sohn, S.J. Lalama, Second harmonic generation in poled polymer films, Appl. Phys. Lett. 49 (1986) 248–250.

[8] S. Yilmaz, S. Bauer, R. Gerhard-Multhaupt, Photothermal poling of nonlinear optical polymer films, Appl. Phys. Lett. 64 (1994) 2770–2772.

[9] A. Chen, V. Chuyanov, S. Ganner, W.H. Steier, Fast maskless fabrication of electrooptic polymer devices by simultaneous direct laser writing and electric poling of channel waveguides, WCC3, LEOS'97 Conference Proceedings (Nov. 1997).

[10] S. Kobayashi, Thermophysical Properties Handbook, Yokendo, 1990 (in Japanese).

[11] J.W. Wu, Birefringent and electro-optic effects in poled polymer films: steady-state and transient properties, J. Opt. Soc. Am. B 8 (1991) 142–152.

[12] L.Y. Lin, D. Remkrishna, H.S. Lackritz, Rotational Browian motion of chromophores and electric field effects in polymer films for second-order nonlinear optics, Macromolecules 27 (1994) 5987–5999.

[13] M.A. Firestone, M.A. Ratner, T.J. Marks, Electric field poling in polymeric nonlinear optical materials, Relaxation Dyn., Model, Exp. Macromolecules 28 (1995) 6296–6310.

[14] G. Arfken, Mathematical Methods for Physicists, Academic Press, San Diego, 1985.

[15] M. Doi, S.F. Edwards, The Theory of Polymer Dynamics, Clarendon Press, Oxford, 1986.

[16] P.N. Prasad, D.J. Williams, Introduction to Nonlinear Optical Effects in Molecules and Polymers, Wiley, New York, 1991, pp. 68–70.